

dc-current transport and ac Josephson effect in quantum junctions at low voltage

E. N. Bratus', V. S. Shumeiko, and E. V. Bezuglyi

*Department of Applied Physics, Chalmers University of Technology and Göteborg University, S-41296 Göteborg, Sweden
and B. Verkin Institute for Low Temperature Physics and Engineering, 47 Lenin Avenue, 310164 Kharkov, Ukraine*

G. Wendin

*Department of Applied Physics, Chalmers University of Technology and Göteborg University, S-41296 Göteborg, Sweden
(Received 30 December 1996)*

Multiple Andreev scattering in single-mode superconducting junctions with arbitrary normal electron transparency $0 < D < 1$ is studied in the limit of low applied voltage $eV \ll \Delta$. A quasiclassical approach is developed for investigation of the dense lattice of inelastic sidebands associated with multiple Andreev scattering, which gives a global description of inelastic-scattering amplitudes and spectral distribution of the current. The cross-over from the contact to the tunnel regime is investigated for the dc current and ac Josephson current as function of junction transparency and applied voltage. A mesoscopic interference effect in junctions with intermediate transparency is discussed. This effect shows up in oscillating features of the current of thermal excitations. [S0163-1829(97)06418-7]

I. INTRODUCTION

During the last 15 years significant effort has been directed towards understanding the physical processes in biased superconducting junctions at applied voltages smaller than the gap value, $eV < 2\Delta$ (Refs. 1–7). The interest in the problem is due to the fact that single-particle current transport at zero temperature is entirely blocked at subgap voltage,⁸ and that the current has multiparticle origin.⁹ Considerable subgap current is systematically observed in experiment, especially in transparent junctions, manifesting a pronounced subharmonic gap structure.^{10–14} The multiparticle mechanism of subgap transport has been found to be closely related to Andreev processes of electron-hole conversions in the junction^{1,4} and to the formation of Andreev bound states within the superconducting energy gap.¹⁵

The progress during the last few years has been due to careful investigations of quantum point contacts. Such structures are available in real experiments on break-junction devices^{16,17} and on gated superconductor-semiconductor devices.¹⁸

In quantum point contacts the problem of subgap current is presented in a refined form. The small size of the junction on the scale of the phase-breaking length, and the separation of transverse electron modes, makes it possible to treat the current through each separate mode in the spirit of the scattering theory approach.^{19,20} The total current through the junction then results from imbalanced currents of quasiparticle scattering states originating from the left and right superconducting electrodes. Quasiparticle scattering in biased superconducting junctions is inelastic because of nonstationary behavior of the superconducting phase difference at the junction. It therefore involves an infinite set of sidebands in the spectrum of scattered waves with energies shifted by an integer number of quanta eV (Ref. 15). Furthermore, some of the sideband states are created within the superconducting gap in the form of Andreev bound states. These states carry current which is converted into supercurrent outside the

junction, providing transmission of Cooper pairs through the junction. Thus, a dc pair current necessarily accompanies the single-particle current of real excitations.

Cancellation of the currents of different inelastic channels, including normal and Andreev current components, is extremely nontrivial. Perturbative analysis of the current in junctions with low normal electron transparency $D \ll 1$ has shown^{15,21} that the normal and Andreev components of the pair current are balanced in a such way that the pair current experiences rapid changes (onsets and spikes) near voltages $eV = 2\Delta/n$. Together with the onsets of the single-particle current this yields the steplike subharmonic gap structure, as shown in Fig. 1. The theoretical results perfectly fit break-junction experimental data without fitting parameters.²² The subharmonic gap structure in quantum junctions with arbitrary transparency has been numerically calculated using different methods in Refs. 4,23,24.

At low applied voltages, $eV \ll \Delta$, the number of inelastic sidebands increases without limit. However, in junctions with small transmissivity, $D \ll 1$, the dc current decays exponentially with decreasing the applied voltage,²⁵ Fig. 1. Very different properties of the dc current have been revealed in the opposite limit of fully transparent junctions, $D = 1$. In this limit, the dc current appears as the average of the time-dependent current associated with adiabatic oscillations of the Andreev bound states, which approaches constant magnitude at low applied voltage,²³ giving rise to a zero-bias peak of the junction conductance.^{7,24}

In this paper we analyze the current through superconducting junctions at low applied voltage $eV \ll \Delta$ in the whole range of junction transparency $0 < D < 1$. Taking advantage of the high spectral density of the sideband lattice, we develop a quasiclassical description of the spectral distribution of the inelastic-scattering amplitudes. This allows us to investigate the global structure of the inelastic scattering amplitudes and the distribution of current among different inelastic channels.

The structure of the paper is the following: in Sec. II we

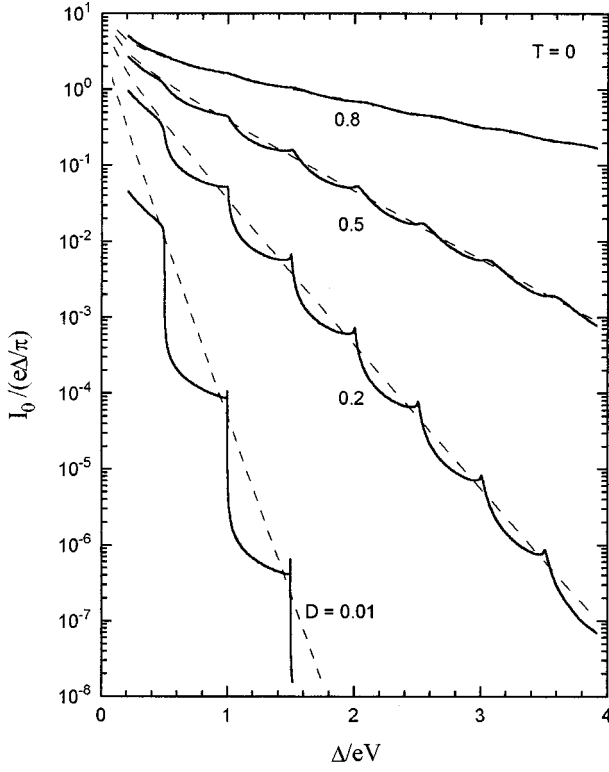


FIG. 1. The subharmonic gap structure of a biased single-mode quantum point contact at zero temperature and at different junction transparencies: $D = 0.01, 0.2, 0.5, 0.8$. The solid lines represent the result of a numerical calculation based on the exact recurrences in Eqs. (3.2a), (3.2b); dashed lines are the analytical result of quasiclassical theory, Eqs. (4.4), (4.5), (4.9).

derive equations for inelastic-scattering amplitudes, while Sec. III is devoted to construction of quasiclassical solutions of these equations. The dc current is calculated in Sec. IV and the ac current is finally discussed in Sec. V.

II. EQUATIONS FOR SCATTERING AMPLITUDES

We consider a superconducting quantum constriction with a local scatterer in the neck (Fig. 2). We assume here that the junction is symmetric, that the constriction is smooth on the scale of the Fermi wavelength, and that there is only a single transport mode. We consider quasiparticle scattering by the junction using the Bogoliubov–de Gennes (BdG) equation²⁷

$$i\dot{\Psi}(t) = \hat{H}\Psi(t) \quad (2.1)$$

with the Hamiltonian

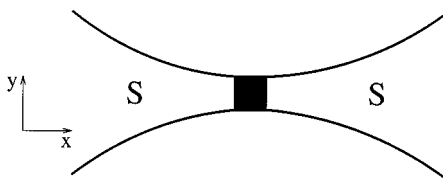


FIG. 2. One-channel adiabatic superconducting constriction. The dark region represents the scatterer with normal electron transparency $0 < D < 1$.

$$\hat{H} = \left[\frac{[\vec{p} - \sigma_z e \vec{A}(\vec{r}, t)]^2}{2m} + V(\vec{r}) - \mu \right] \sigma_z + [U(x) + e\varphi(\vec{r}, t)] \sigma_z + \hat{\Delta}(\vec{r}, t). \quad (2.2)$$

In Eq. (2.2), $V(\vec{r})$ is the potential defining the constriction, $U(x)$ is the potential of the scatterer, $\vec{A}(\vec{r}, t)$ and $\varphi(\vec{r}, t)$ are electromagnetic potentials, and $\hat{\Delta}(\vec{r}, t)$ is the superconducting order parameter given by the matrix

$$\hat{\Delta} = \begin{pmatrix} 0 & \Delta e^{i\chi/2} \\ \Delta e^{-i\chi/2} & 0 \end{pmatrix}. \quad (2.3)$$

σ_z is the Pauli matrix, and the choice of units corresponds to $c = \hbar = 1$.

Due to the adiabatic geometry of the junction,²⁶ we may use the quasiclassical wave functions far from the scatterer,

$$\Psi(\vec{r}, t) = \sum_{\beta} \psi_{\perp}(\vec{r}_{\perp}, x) \frac{1}{\sqrt{v}} e^{i\beta \int p dx} \psi^{\beta}(x, t), \quad (2.4)$$

where $\psi_{\perp}(x), \psi^{\beta}(x)$ are slowly varying functions, ψ_{\perp} is the normalized wave function of the transverse mode, $p = \sqrt{2m(\mu - E_{\perp})}$ is the longitudinal momentum of the quasiclassical electron, $v = p/m$, and $\beta = \pm$ indicates the direction of electron motion. We will also explicitly separate out the phase $\chi(\vec{r}, t)$ of the superconducting order parameter $\hat{\Delta}$ in Eq. (2.3) by means of a gauge transformation

$$\psi^{\beta} \rightarrow e^{i\sigma_z \chi/2} \psi^{\beta}, \quad (2.5)$$

and introduce a superfluid momentum $\vec{p}_s = \nabla \chi/2 - e\vec{A}$ and a gauge-invariant electric potential $\Phi = \dot{\chi}/2 + e\varphi$. The coefficients ψ^{β} in Eq. (2.4) then obey the reduced BdG equation:

$$i\dot{\psi}_{L,R}^{\beta} = (\beta v \hat{p} \sigma_z + \Phi_{L,R} \sigma_z + v p_{sL,R} + \Delta \sigma_x) \psi_{L,R}^{\beta} \quad (2.6)$$

in the left (L) and the right (R) electrodes. Within such an approximation, the local scatterer in the neck of the constriction imposes a boundary condition to Eq. (2.6), which is determined by the normal electron-scattering amplitudes d and r ($|d|^2 + |r|^2 = D + R = 1$, $r/d = -r^*/d^*$). If the scattering amplitudes are energy-independent near the Fermi level, the boundary condition has the form^{21,28}

$$\begin{pmatrix} \psi_L^- \\ \psi_R^+ \end{pmatrix} = \begin{pmatrix} r & d e^{i\sigma_z \phi/2} \\ d e^{-i\sigma_z \phi/2} & r \end{pmatrix} \begin{pmatrix} \psi_L^+ \\ \psi_R^- \end{pmatrix}_{x=0}, \quad (2.7)$$

where ϕ is the gauge-invariant difference of the superconducting phases of the right and left electrodes: $\phi(t) = \chi_R(0, t) - \chi_L(0, t)$.

In the point-contact geometry, the effect of spreading out of the current gives rise to a negligibly small spatial deviation of the order parameter Δ from constant magnitude,²⁹ $\Delta = \text{const}$. For the same reason, practically the whole applied voltage drop V occurs at the junction,³⁰ $\varphi_L - \varphi_R = V$. Neglecting effects of penetration of the electromagnetic field into the superconductor, we omit the potentials p_s and Φ

from Eq. (2.6), $p_s = \Phi = 0$. The relation $\Phi = 0$ yields the Josephson relation between the phase difference and the applied voltage, $\dot{\phi} = 2eV$.

In view of the time dependence of the boundary condition in Eq. (2.7), the scattering states are to be constructed from the eigenstates of Eq. (2.6) for different energies $E_n = E + neV$, shifted with respect to the energy E of the incoming wave by an integer multiple of eV , $-\infty < n < \infty$. The wave functions of the scattering states, calculated at the midpoint of the junction ($x=0$), have the form

$$\begin{pmatrix} \psi_L^- \\ \psi_R^+ \end{pmatrix}_{jE} = \begin{pmatrix} \delta_{j,1} \\ \delta_{j,2} \end{pmatrix} \frac{u_E^-}{\sqrt{E}} e^{-iEt} + \sum_n \begin{pmatrix} a \\ b \end{pmatrix}_{jn} u_n^+ e^{-iE_n t}, \quad (2.8)$$

$$\begin{pmatrix} \psi_L^+ \\ \psi_R^- \end{pmatrix}_{jE} = \begin{pmatrix} \delta_{j,3} \\ \delta_{j,4} \end{pmatrix} \frac{u_E^+}{\sqrt{E}} e^{-iEt} + \sum_n \begin{pmatrix} c \\ f \end{pmatrix}_{jn} u_n^- e^{-iE_n t},$$

where $j=1-4$ labels scattering states having the same incoming energy E . In Eqs. (2.8) u_n is solution of the homogeneous BdG equation,

$$u_n^\pm = \frac{1}{\sqrt{2}} \begin{pmatrix} e^{\pm \gamma_n/2} \\ \sigma_n e^{\mp \gamma_n/2} \end{pmatrix}, \quad (2.9)$$

$$e^{\gamma_n} = \frac{|E_n| + \xi_n}{\Delta}, \quad \sigma_n = \text{sgn}(E_n),$$

$$\xi_n = \begin{cases} \sqrt{E_n^2 - \Delta^2}, & |E_n| > \Delta \\ i\sigma_n \sqrt{\Delta^2 - E_n^2}, & |E_n| < \Delta \end{cases}$$

Combination of Eqs. (2.7)–(2.9) yields equations for the scattering amplitudes which reduce to a closed set of recurrences for the transmission amplitudes. For example, for a holelike quasiparticle incoming from the left ($j=1$), the recurrences read

$$\begin{pmatrix} b_{n+1} \\ f_{n+1} \end{pmatrix} = \hat{M}_n \begin{pmatrix} b_{n-1} \\ f_{n-1} \end{pmatrix} - \frac{2e^{\gamma_0/2} \sinh \gamma_0}{d\sqrt{E}} \begin{pmatrix} r e^{-\gamma_1/2} \\ e^{\gamma_1/2} \end{pmatrix} \delta_{n,0}, \quad (2.10)$$

where the matrix \hat{M}_n has the form

$$\hat{M}_n = \sigma_n \sigma_{n-1} \begin{pmatrix} (e^{\gamma_n} - (2/D) \sinh \gamma_n) e^{-(\gamma_{n+1} + \gamma_{n-1})/2} & (2r/D) \sinh \gamma_n e^{-(\gamma_{n+1} - \gamma_{n-1})/2} \\ (-2r^*/D) \sinh \gamma_n e^{(\gamma_{n+1} - \gamma_{n-1})/2} & (e^{-\gamma_n} + (2/D) \sinh \gamma_n) e^{(\gamma_{n+1} + \gamma_{n-1})/2} \end{pmatrix}, \quad (2.11)$$

and where

$$\text{Det} \hat{M}_n = 1.$$

The transmission amplitudes of the other scattering states $j=2-4$ satisfy similar equations and are related to the solution of equations (2.10), (2.11) through the symmetry relations

$$\begin{pmatrix} b_{3n} \\ f_{3n} \end{pmatrix}(\gamma, r, d) = \begin{pmatrix} f_n \\ b_n \end{pmatrix}(-\gamma, r^*, d^*), \quad (2.12a)$$

$$\begin{pmatrix} c_{2n} \\ a_{2n} \end{pmatrix}(\gamma) = \sigma_0 \sigma_n \begin{pmatrix} f_n \\ b_n \end{pmatrix}(-\gamma). \quad (2.12b)$$

The relation between the amplitudes of the scattering states $j=4$ and $j=2$ is similar to Eq. (2.12a).

The charge current associated with a single scattering state is given by the standard quantum-mechanical formula

$$I_{jE}(x, t) = \frac{e}{2m} \left\{ (\hat{p} - \hat{p}') \int d^2 r_\perp (\Psi(\vec{r}', t), \Psi(\vec{r}, t)) \right\}_{\vec{r}=\vec{r}'}. \quad (2.13)$$

The brackets in Eq. (2.13) denote a scalar product in electron-hole space. Eq. (2.13) is a particular form of a general equation for the charge current in nonequilibrium superconductors derived, e.g., in Ref. 31. In the quasiclassical approximation of Eq. (2.4) the current (2.13), calculated at the junction has form

$$I_{jE}(\pm 0, t) = e \sum_\beta \beta |\psi_{jE}^\beta(\pm 0, t)|^2. \quad (2.14)$$

The current in Eq. (2.14) can be calculated at either side of the junction: identity of the both expressions is guaranteed by the unitarity of the matching matrix in Eq. (2.7).

The wave function $\Psi(t)$ in Eq. (2.1) describes evolution in time of a quasiparticle state which originates from an eigenstate of the homogeneous BdG equation. According to the assumption of local equilibrium in the electrodes, a quasiparticle distribution among the eigenstates corresponds to the Fermi distribution. The total current results from Eq. (2.14) after summation over all quantum numbers of the incoming states, $|E| > \Delta$, $j=1-4$, with account of the Fermi filling factors. Expressing partial transmitted currents of individual scattering states in Eq. (2.14) through the scattering amplitudes, and making use of relations (2.12) and the symmetry relations

$$b_n(-E, \gamma, r, d) = \sigma_n b_{-n}^*(E, -\gamma, r^*, d^*), \quad (2.15)$$

$$f_n(-E, \gamma, r, d) = \sigma_n f_{-n}^*(E, -\gamma, r^*, d^*),$$

we finally arrive at an equation for the total current,

$$I(t) = \frac{e}{\pi N} \sum_{N=-\infty}^{\infty} e^{i2NeVt} \int_{\Delta}^{\infty} \frac{dE E}{\xi} \tanh(E/2T) \sum_{n=\text{odd}} K_{n+2N, n}, \quad (2.16)$$

where

$$K_{nm} = (1/2)(1 + \sigma_n \sigma_m) \{ [(u_n^-, u_m^-) f_n^* f_m - (u_n^+, u_m^+) b_n^* b_m] - [\gamma \rightarrow -\gamma] \}. \quad (2.17)$$

When deriving Eq. (2.17) we have taken into account the fact that the products of scattering amplitudes $f_n^* f_m$ and $b_n^* b_m$ depend on the scattering probabilities D and R rather than on the scattering amplitudes d and r [see below Eqs. (3.2), (3.3)].

The form of the recurrences in Eq. (2.10), together with equation Eq. (2.17) for the current spectral density, allows us to make an important observation. The matrix elements in Eq. (2.11) are related, for all n , as

$$M_{11}(\gamma) = M_{22}(-\gamma), \quad M_{12}(\gamma, r) = M_{21}(-\gamma, r^*). \quad (2.18)$$

Within the superconducting gap the quantities γ_n in Eq. (2.9) are imaginary, and the symmetry relations in Eq. (2.18) take the form

$$\hat{M}_n \sigma_z \hat{M}_n^\dagger = \sigma_z. \quad (2.19)$$

This generates a conservation law

$$|b_n|^2 - |f_n|^2 = \text{const}, \quad |E_n| < \Delta, \quad (2.20)$$

which imposes a constant distribution of the time-independent current ($N=0$) of *each scattering state* among the Andreev bound states.

III. QUASICLASSICAL SOLUTIONS

Although a formal solution of the homogeneous equation in Eq. (2.10) is easily obtained:

$$\begin{pmatrix} b_{2n+1} \\ f_{2n+1} \end{pmatrix} = \prod_{k=1}^{k=n} \hat{M}_{2k} \begin{pmatrix} b_1 \\ f_1 \end{pmatrix}, \quad (3.1)$$

this is not very helpful because in junctions with arbitrary transparency $D \neq 1$, the matrices \hat{M}_n do not commute and the product in Eq. (3.1) cannot be calculated analytically. The exception is a perfect constriction, $R=0$, where the matrices \hat{M}_n are diagonal and explicit calculation of the scattering amplitude is possible.²⁵ In the limit of low voltage, $eV/\Delta \ll 1$, the matrices \hat{M}_n change slowly with n and nearly commute if their indices are close to each other, which allows application of the two-scale expansion technique for approximate calculation of the product.

In this paper we will use another way of approximate calculation. We split the matrix equation (2.10) into two independent second-order difference equations

$$A_n^+ f_{n+2} + A_n^- f_{n-2} + A_n f_n = - \frac{2 \sinh \gamma_n}{d \sqrt{E/\Delta}} (e^{-(\gamma_0 + \gamma_1)/2} \delta_{n,1} - \sigma_0 \sigma_{-1} e^{(\gamma_0 + \gamma_{-1})/2} \delta_{n,-1}), \quad (3.2a)$$

$$\begin{aligned} \bar{A}_n^+ b_{n+2} + \bar{A}_n^- b_{n-2} + \bar{A}_n b_n &= \frac{2r \sinh \gamma_n}{d \sqrt{E/\Delta}} (e^{(\gamma_1 - \gamma_0)/2} \delta_{n,1} \\ &\quad - \sigma_0 \sigma_{-1} e^{(\gamma_0 - \gamma_{-1})/2} \delta_{n,-1}), \end{aligned} \quad (3.2b)$$

where the coefficients are given by

$$\begin{aligned} A_n^+ &= -\sigma_n \sigma_{n+1} e^{(\gamma_n - \gamma_{n+2})/2} \frac{\sinh \gamma_n}{\sinh \gamma_{n+1}}, \\ A_n^- &= -\sigma_{n-1} \sigma_{n-2} e^{(-\gamma_n + \gamma_{n-2})/2} \frac{\sinh \gamma_n}{\sinh \gamma_{n-1}}, \\ A_n &= \frac{4}{D} \sinh^2 \gamma_n + e^{\gamma_n - \gamma_{n+1}} \frac{\sinh \gamma_n}{\sinh \gamma_{n+1}} + e^{-\gamma_n + \gamma_{n-1}} \frac{\sinh \gamma_n}{\sinh \gamma_{n-1}}, \end{aligned} \quad (3.3)$$

$$\bar{A}(\gamma) = A(-\gamma).$$

Then, taking advantage of the short period of the sideband lattice and the slow variation of the coefficients in Eqs. (3.3), we transform the difference equations (3.2) into differential equations and apply the familiar technique of the quasiclassical approximation. Such a method allows us to calculate current-voltage characteristics in the whole range of junction transparency $0 < D < 1$. However, in the I - V characteristics obtained with this method the subharmonic gap structure is lost because the sideband lattice is washed out (this is illustrated in Fig. 1).

Below we will use dimensionless quantities $E/\Delta, E_n/\Delta \rightarrow E, E_n$. Expanding (the homogeneous) equation (3.2a) from the lattice E_n , $n = \text{odd}$ to the continuous axis, $E_n \rightarrow \epsilon$, and keeping the nonlocality of the coefficients (3.3) to first order in eV/Δ , we arrive at the following equation:

$$\begin{aligned} &\left[\left(1 - \frac{\omega}{2} \gamma'(\alpha + \coth \gamma) \right) e^{\omega d/\epsilon} \right. \\ &\quad \left. + \left(1 - \frac{\omega}{2} \gamma'(\alpha - \coth \gamma) \right) e^{-\omega d/\epsilon} \right. \\ &\quad \left. - 2U(\epsilon) + \alpha \omega \gamma' \right] f(\epsilon) = 0, \end{aligned} \quad (3.4)$$

$$U(\epsilon) = 1 + (2/D)(\epsilon^2 - 1).$$

In Eq. (3.4), $\omega = 2eV/\Delta$ is the dimensionless Josephson frequency, $\gamma' = d\gamma/d\epsilon$, and the index $\alpha = \pm$ is introduced in order to keep trace of both solutions with $\pm \gamma$, necessary for calculation of the current in Eqs. (2.16), (2.17). Equation (3.4) is valid on the whole axis ϵ except of the point $\epsilon=0$ where the coefficients A^\pm in Eq. (3.3) have a discontinuity in the limit $\omega \rightarrow 0$. This results in discontinuity of the function f , which can be taken into account by multiplying the continuous solution \tilde{f} of Eq. (3.4) by a discontinuity factor,

$$f(\epsilon) = e^{i\alpha(\pi/2)\theta(\epsilon)} \tilde{f}(\epsilon). \quad (3.5)$$

Equation (3.4) in the classical limit $\omega \rightarrow 0$ has a simple physical interpretation: it describes one-dimensional motion of a particle with the dispersion law $\cos \omega \tau$ in the potential

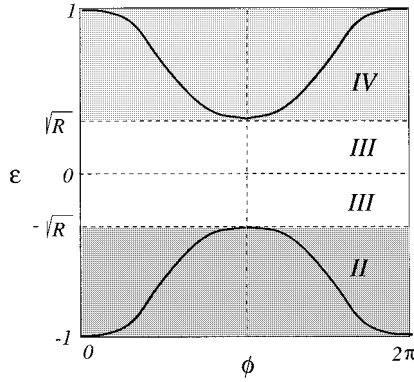


FIG. 3. Energy-phase diagram of static Andreev bound-state bands $\epsilon(\phi)$.

$-U(\epsilon)$, $\cos\omega\tau - U(\epsilon) = 0$. This motion corresponds to adiabatic oscillations of the Andreev bound states^{28,32,33} in a voltage-biased junction:

$$\epsilon(\phi) = \pm \sqrt{1 - D \sin^2[\phi(\tau)/2]}, \quad \phi(\tau) = \omega\tau, \quad \tau = \Delta t. \quad (3.6)$$

Furthermore, Eq. (3.6) determines classically allowed regions in Eq. (3.4) which coincide with the position of the static Andreev bound bands $\epsilon(\phi)$, $\sqrt{R} < |\epsilon| < 1$, Fig. 3. The energy gap between the Andreev bands, $|\epsilon| < \sqrt{R}$, together with the continuum spectrum, $|\epsilon| > 1$, constitute forbidden regions. Applicability of the quasiclassical approximation requires that the size of each region is much larger than the spacing of the sideband lattice,

$$\min(D, \sqrt{R}) \gg \omega. \quad (3.7)$$

The wave equation (3.4) gives a description of the dynamics of the Andreev bound states in an energy domain which is complementary to the time-domain description developed in Ref. 23; it allows us to treat nonadiabatic effects of Andreev bound-state dynamics. The quasiclassical solution of Eq. (3.4) reads

$$\tilde{f}_{\pm}(\epsilon_0, \epsilon) = \left| \frac{D}{\epsilon^2 - R} \right|^{1/4} e^{\pm S_{\alpha}(\epsilon_0, \epsilon)}. \quad (3.8)$$

In classically allowed regions (regions II and IV in Figs. 3 and 4), the quasiclassical exponent S_{α} has the form

$$S_{\alpha}(\epsilon_0, \epsilon) = \int_{\epsilon_0}^{\epsilon} d\epsilon' \left(\frac{i}{\omega} \arccos U(\epsilon') + \frac{\alpha}{2\sqrt{\epsilon'^2 - R}} \right), \quad \sqrt{R} < |\epsilon| < 1. \quad (3.9a)$$

In the forbidden regions outside the superconducting energy gap (regions I and V–VI), the quasiclassical exponent S_{α} reads

$$S_{\alpha}(\epsilon_0, \epsilon) = \int_{\epsilon_0}^{\epsilon} d\epsilon' \left(\frac{1}{\omega} \operatorname{arccosh} U(\epsilon') - \frac{\alpha \operatorname{sgn} \epsilon'}{2\sqrt{\epsilon'^2 - R}} \right), \quad |\epsilon| > 1, \quad (3.9b)$$

while within the Andreev gap (region III)

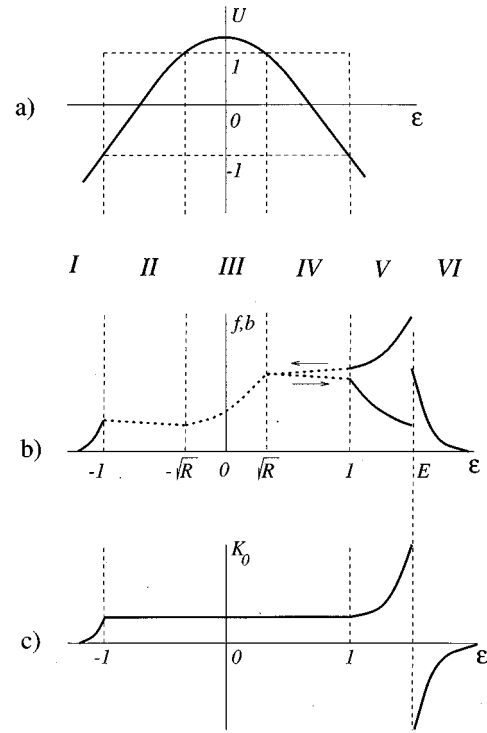


FIG. 4. Scattering state on the energy axis: (a) effective potential; (b) solution of Eq. (3.4): the dotted line represents an envelope of rapidly oscillating wave function; in regions IV–V the incoming and the reflected waves are shown separately, indicated by arrows; (c) spectral distribution of the dc current, which is constant inside the gap due to compensation of normal (f) and Andreev (b) current channels; this compensation is absent in regions V, VI.

$$S_{\alpha}(\epsilon_0, \epsilon) = \int_{\epsilon_0}^{\epsilon} d\epsilon' \left(\frac{1}{\omega} [i\pi - \operatorname{arccosh}|U(\epsilon')|] + \frac{\alpha i}{2\sqrt{R - \epsilon'^2}} \right), \quad |\epsilon| < \sqrt{R}. \quad (3.9c)$$

In Eqs. (3.8), (3.9) only the main branch of the function $\phi(\epsilon)$ in Eq. (3.6) is used, since we are only interested in the values of $\tilde{f}(\epsilon)$ on the lattice $\epsilon = E_n$ where all branches give the same magnitude of \tilde{f} .

It is interesting to note the role of small nonadiabatic (proportional to ω) corrections to the coefficients of equation (3.4). These terms contribute to the pre-exponential factors in the quasiclassical solutions and cannot be neglected. Containing an imaginary part, they cause violation of the conservation of the probability current in Eq. (3.4); this leads to specific interference effects in the spectral distribution of the inelastic-scattering amplitudes [see below Eq. (4.6) and following discussion]. Also, they cause suppression of reflection at the edges of the superconducting gap $|\epsilon| = 1$, which are the singular points of the quasiclassical solutions.

Indeed, in the vicinity of the gap edge points $\epsilon = \pm 1$, Eq. (3.4) reduces to

$$\omega^2 f'' - \frac{\omega^2}{2(\epsilon \mp 1)} f' \mp \frac{8}{D} (\epsilon \mp 1) f = 0,$$

the exact solution of which, $f = \exp[\pm(4/3)\sqrt{2/D}\omega^2(\pm\epsilon-1)^{3/2}]$, does not contain any reflected wave. Thus, the matching conditions at the superconducting gap edges are determined by analytic continuation of the exponents S_α in Eqs. (3.9):

$$f_\pm^I(-1, \epsilon) \rightarrow f_\pm^{II}(-1, \epsilon), \quad (3.10)$$

$$f_\pm^V(1, \epsilon) \rightarrow f_\pm^{IV}(1, \epsilon).$$

In contrast to the superconducting gap edges, the edges of the Andreev gap, $\epsilon = \pm\sqrt{R}$, are true turning points. To derive the matching conditions at these points we first separate out

$$\begin{pmatrix} C_+^{III} \\ C_-^{III} \end{pmatrix} = \begin{pmatrix} (1/2)e^{i\pi/4} \\ e^{-i\pi/4+2\pi i(E+\sqrt{R})/\omega} \end{pmatrix} \begin{pmatrix} C_+^{II} \\ C_-^{II} \end{pmatrix} \quad (3.12)$$

between the coefficients of linear combinations

$$f(\epsilon) = C_+ f_+(\epsilon_0, \epsilon) + C_- f_-(\epsilon_0, \epsilon) \quad (3.13)$$

in regions *III* and *II* (the quasiclassical exponents are here counted from the boundary $\epsilon_0 = -\sqrt{R}$). The matching equation (3.12) takes into account exponentially small terms in the asymptotics of the Airy functions in the under-the-barrier region,³⁴ which is necessary for consistency with the conservation law (2.20). The solutions in regions *III* and *IV* are related in a similar way. Combining both matching equations with the solution inside the Andreev gap, $-\sqrt{R} < \epsilon < \sqrt{R}$, we find a direct relation between the coefficients C_\pm in Eq. (3.13) in the allowed regions *II* and *IV*,

$$\begin{pmatrix} C_+^{IV} \\ C_-^{IV} \end{pmatrix} = \hat{t} \begin{pmatrix} C_+^{II} \\ C_-^{II} \end{pmatrix}, \quad (3.14)$$

where transfer matrix \hat{t} has elements

$$t_{12} = t_{21}^* = i(e^\Phi + e^{-\Phi}/4)e^{-2\pi i E/\omega}, \quad (3.15)$$

$$t_{11} = t_{22}^* = (e^\Phi - e^{-\Phi}/4)e^{2\pi i \sqrt{R}/\omega},$$

$$\text{Det} \hat{t} = -1,$$

$$\Phi = \frac{1}{\omega} \int_{-\sqrt{R}}^{\sqrt{R}} d\epsilon \operatorname{arccosh}|U(\epsilon)|.$$

If the Andreev gap is narrow, $R \ll D\omega^{1/3}$, and the turning points are not well separated, the transfer matrix \hat{t} is found directly from equation (3.11),

$$t_{12} = t_{21}^* = i e^{\pi R/\omega - 2\pi i E/\omega}, \quad (3.16)$$

$$\begin{aligned} t_{11} = t_{22}^* &= \sqrt{R/2\pi\omega} \Gamma(iR/\omega) (1 - e^{2\pi R/\omega}) e^{-\pi R/2\omega} \\ &\times \exp(-iR/\omega) [1 + \ln(\omega/R)] \\ &- 2\pi i \sqrt{R/\omega} - \pi i/4, \end{aligned}$$

rapid oscillations of the solutions by introducing $\tilde{f} = e^{i\pi\epsilon/\omega} g$. Then Eq. (3.4) reduces to a parabolic cylinder equation in the vicinity of each turning point,

$$\omega^2 g'' + \left[\frac{4}{D}(\epsilon^2 - R) + \frac{2i\alpha\omega}{\sqrt{D}} \right] g = 0. \quad (3.11)$$

If the turning points are well separated, $R \gg D\omega^{1/3}$, Eq. (3.11) further reduces to the Airy equation. Then the standard matching procedure carried out, e.g., at the point $\epsilon = -\sqrt{R}$, yields the relation

where Γ is the Γ function and $\text{Det} \hat{t} = -1$.

The off-diagonal matrix element t_{12} of the transfer matrix \hat{t} has the meaning of inverse amplitude of tunneling through the Andreev gap. The probability of tunneling $W = |t_{12}|^{-2}$ resulting from Eq. (3.15) is

$$W = e^{-2\Phi} = \begin{cases} e^{-\pi\Delta R/eV}, & R \ll 1, \\ e^{(2\Delta/eV)\ln(D/16)}, & D \ll 1. \end{cases} \quad (3.17)$$

In the high transparency limit $R \ll 1$ the result (3.17) coincides with the tunneling probability that follows directly from Eq. (3.16).

Evaluation of the coefficients C_\pm in all regions is completed by taking into account the boundary condition at infinity, $f(\pm\infty) = 0$, and the source term in Eq. (3.2). Assuming in Eq. (3.2a)

$$f_{-2k-1} = A\lambda^k + B\lambda^{-k}, \quad f_{2k+1} = C^{VI}\lambda^{-k}, \quad (3.18)$$

for $k=0,1$ with $\lambda = \exp[\operatorname{arccosh}U(E)]$, and neglecting the variation of the coefficients with n , we find

$$B = \frac{\xi}{d}(\sqrt{D} + \alpha), \quad C^{VI} - A = \frac{\xi}{d}(\sqrt{D} - \alpha), \quad \xi \ll D. \quad (3.19)$$

The explicit form of the coefficients C_\pm in all regions for different choices of boundaries ϵ_0 is presented in Table I.

Calculation of the scattering amplitudes b in Eq. (3.2b) is carried out in a similar way. This leads to the equations

$$B = \frac{\alpha\xi r}{d}, \quad C_-^{VI} = \frac{t_{22}}{t_{12}} B e^{-2S_{-\alpha}(\sqrt{R}, \epsilon)} - \frac{\alpha\xi r}{d}. \quad (3.20)$$

The other coefficients in regions *I–VI* have the same analytical form as the ones in Table I, the coefficient B being given by Eq. (3.20) and the exponent $S_{-\alpha}$ substituting for S_α .

TABLE I. Reference points ϵ_0 and coefficients C_{\pm} of linear form in Eq. (3.13) for quasiclassical solutions of wave equation (3.4) for transmitted amplitude f in different regions $I-VI$.

	ϵ_0	C_+	C_-
I	-1	$\frac{B}{t_{12}} e^{-2S_{\alpha}(\sqrt{R},1)-S_{\alpha}(1,E)}$	0
II	$-\sqrt{R}$	0	$\frac{B}{t_{12}} e^{-S_{\alpha}(\sqrt{R},E)}$
III	$-\sqrt{R}$	$\frac{B}{2t_{12}} e^{-S_{\alpha}(\sqrt{R},E)} e^{-\pi i/4-2\pi i(E+\sqrt{R})/\omega}$	$\frac{B}{t_{12}} e^{-S_{\alpha}(\sqrt{R},E)} e^{\pi i/4}$
IV	\sqrt{R}	$B e^{-S_{\alpha}(\sqrt{R},E)}$	$\frac{t_{22}}{t_{12}} B e^{-S_{\alpha}(\sqrt{R},E)}$
V	1	$B e^{-S_{\alpha}(1,E)}$	$\frac{t_{22}}{t_{12}} B e^{-2S_{\alpha}(\sqrt{R},1)-S_{\alpha}(1,E)}$
VI	E	0	$\frac{t_{22}}{t_{12}} B e^{-2S_{\alpha}(\sqrt{R},E)} + \frac{\xi}{d} (\sqrt{D}-\alpha)$

The solutions found above resemble scattering states of a quantum particle propagating along the energy axis through a potential barrier, related to the gap between Andreev bound bands as illustrated in Fig. 4. The amplitude of the incoming wave is determined at the injection point $\epsilon = E$ by the source terms in Eqs. (3.2). Decaying towards the superconducting gap edge, the incoming wave transforms without reflection into a propagating wave within the superconducting gap. Approaching the Andreev gap, it is partially reflected and partially transmitted through the Andreev gap with probability W into the other Andreev band. Then, after approaching the other superconducting gap edge at $\epsilon = -1$, it finally decays outside the superconducting gap. The condition of wavefunction decay at infinity plays the role of the outgoing condition in conventional scattering problems determining transmitted and reflected waves. Such a scattering state along the E axis gives a complete description of the spectral distribution of inelastic-scattering amplitudes of the original scattering problem—it therefore provides a basis for calculation of the current through the junction.

IV. TIME-INDEPENDENT CURRENT

In this section we evaluate the time-independent component of the current. This current consists of the sum of incoherent contributions, $N=0$, of all the sidebands in Eq. (2.16). Assuming that the current spectral density K_{nn} varies slowly with sideband index n , we approximate the sum over n with the integral along ϵ ,

$$I_0 = \frac{e\Delta}{\pi} \int_1^{\infty} \frac{dE E}{\xi} \tanh(E\Delta/2T) \int_{-\infty}^{\infty} \frac{d\epsilon}{\omega} K_0(E, \epsilon), \quad (4.1)$$

$$K_0(E, \epsilon) = \cosh[\text{Re}\gamma(\epsilon)] \{ |f(E, \epsilon)|^2 - |b(E, \epsilon)|^2 \} - (\gamma \rightarrow -\gamma).$$

We will distinguish three components in the averaged current: single-particle current of the real excitations $I_{<}$ (region I , $\epsilon < -1$), pair current of the Andreev bound states I_{Δ} (re-

gions $II-IV$, $-1 < \epsilon < 1$), and current of the ground-state modes $I_{>}$ (regions $V-VI$, $\epsilon > 1$),

$$I_0 = I_{<} + I_{\Delta} + I_{>}. \quad (4.2)$$

According to the conservation law Eq. (2.20), the current spectral density K_0 does not depend on ϵ within the superconducting gap, $K_0(\epsilon) = \text{const}$ (Fig. 4). K_0 is easily evaluated at superconducting gap edge $\epsilon = -1$,

$$K_0(E, |\epsilon| < 1) = K_0(E, -1) = \frac{4\xi^2 W}{\sqrt{D}} e^{-2S(1,E)}. \quad (4.3)$$

Thus the current spectral density is exponentially small *everywhere within the superconducting gap* if $R > \omega$, i.e., for sufficiently low voltage [cf. Eq. (3.17)]. Multiplying equation (4.3) by 2, the size of the gap region, and performing integration over energy E , we get

$$I_{\Delta} = \frac{2e\Delta W}{\pi} \tanh(\Delta/2T). \quad (4.4)$$

This current gives the main contribution to the time-independent current at zero temperature. We notice, that the voltage dependence enters Eq. (4.4) only through the tunneling probability W , while the large pre-exponential factor ω^{-1} in Eq. (4.1) related to the large number of Andreev bound states is compensated for by a small phase volume of relevant scattering states, $E-1 \sim (D\omega^2)^{1/3}$. In accordance with the voltage dependence of W in Eq. (3.17), the current in Eq. (4.4) undergoes crossover from the contact to the tunnel regime at $eV \approx \pi R\Delta$ (cf. Refs. 23,25), as shown in Fig. 5.

The current spectral density K_0 rapidly decays with departure from the energy gap into region I and is concentrated

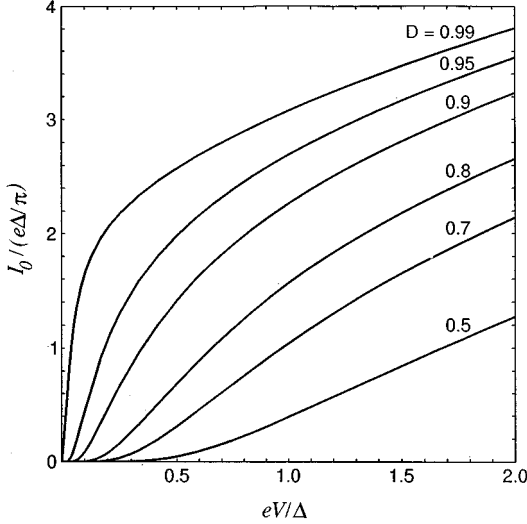


FIG. 5. Current I_0 vs applied voltage at different junction transparencies.

in a narrow interval $\epsilon + 1 \sim (D\omega^2)^{1/3}$. This yields a small magnitude of the current of real excitations $I_<$ in comparison with the pair current $I_Δ$,

$$I_< = \frac{e\Delta W}{2\pi} a(D\omega^2)^{1/3} \tanh(\Delta/2T), \quad (4.5)$$

$$a = \Gamma(2/3)/6^{1/3} = 0.742.$$

Let us now discuss the currents in regions V–VI:

$$K_0^V(E, \epsilon) = \frac{4\xi^2}{\sqrt{D}} e^{-2S(1,E)} (e^{2S(1,\epsilon)} - |Q|^2 e^{-2S(1,\epsilon)}) \quad (4.6a)$$

$$K_0^{VI}(E, \epsilon) = -\frac{4\xi^2}{\sqrt{D}} e^{-2S(1,\epsilon)} (e^{2S(1,E)} + |Q|^2 e^{-2S(1,E)} - 2\sqrt{R}ReQ). \quad (4.6b)$$

The quantity

$$Q = \frac{t_{22}}{t_{12}} \exp\left(-\frac{2i}{\omega} \int_{\sqrt{R}}^1 \arccos V dE\right), \quad (4.7)$$

in Eqs. (4.6) has the meaning of the amplitude of reflection from the superconducting gap. The ratio

$$t_{22}/t_{12} = \sqrt{1 - W} e^{-i\pi/2 + (2i\pi/\omega)(E - \sqrt{R})} \quad (4.8)$$

is the reflection amplitude caused by the Andreev gap, and the oscillating factor in Eq. (4.7) contains the additional phase gained during propagation through the region IV. Thus the first terms in the brackets in Eqs. (4.6) correspond to the currents of incoming and reflected waves while the third term in Eq. (4.6b) is the interference current.

In contrast to regions I–IV, the current spectral densities K_0^V and K_0^{VI} are not exponentially small (Fig. 4). However, at zero temperature one should expect very precise cancellation of these currents since the imbalance effect is only produced by the creation of a tiny amount of real excitations. Indeed,

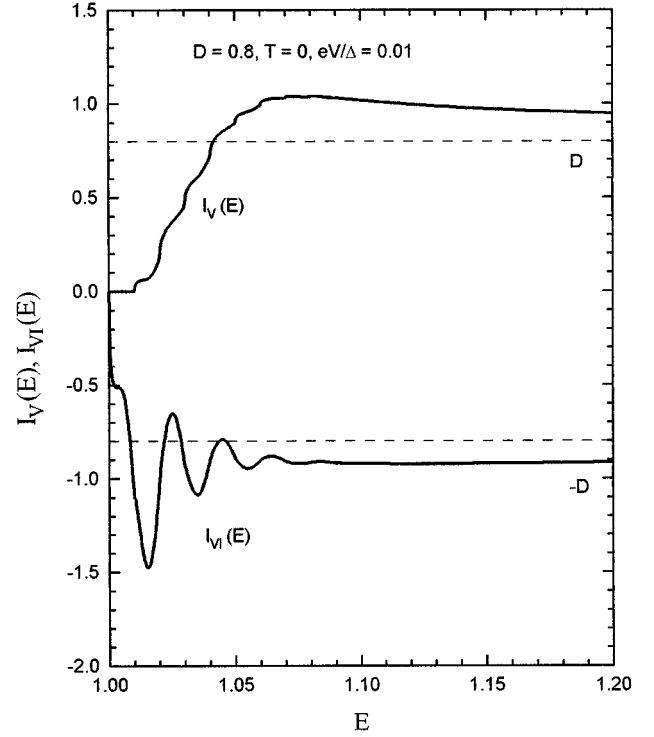


FIG. 6. Currents in regions V–VI calculated from the exact recurrences (2.10); currents $I_V(E)$ and $I_{VI}(E)$ represent current densities K_0^V and K_0^{VI} from Eq. (4.6) respectively, integrated over ϵ . The current I_{VI} reveals pronounced oscillations vs E reflecting the interference term in Eq. (4.6b), while the interference effect in I_V is much smaller. The asymptotics at large E correspond to the current spectral density in the normal junctions.

the dissipative current I_0 determines the rate $\dot{\mathcal{E}}$ of energy transfer from the external source to the electron system: $\dot{\mathcal{E}} = VI_0$. This energy is expended for creation of real excitations; it consists of the product of energy 2Δ lost to single excitation, the tunneling probability W , and the frequency of attempts eV : $\dot{\mathcal{E}} \sim 2\Delta WeV$. This rough estimate yields $I_0 \sim I_Δ$. Direct calculation of noninterference currents in Eqs. (4.6) supports the above conclusion: the currents of regions V–VI compensate each other with exponential accuracy after integration over energy E , giving the result

$$I_> = \frac{e\Delta W}{2\pi} a(D\omega^2)^{1/3}. \quad (4.9)$$

This coincides with the current of real excitations $I_<$, Eq. (4.5). At the same time, the interference current is not canceled but yields a residual oscillating current which is not exponentially small. This result apparently contradicts the above arguments (exponentially small I_0) and also the result of exact numerical calculation of the subharmonic gap structure in Fig. 1, which does not show any background current in the limit of low voltage.

The correct behavior is revealed by detailed numerical investigation of the currents in regions V–VI carried out on the basis of the exact recurrences in Eq. (2.10). In Fig. 6, the currents $I_V(E)$ and $I_{VI}(E)$ show the integral contribution of the regions V and VI [the current densities in Eqs. (4.6)

integrated over $\epsilon]$. The current in region VI shows pronounced interference oscillations similar to our analytical result in Eq. (4.6b). The current in region V also possesses an oscillating component but with much smaller amplitude. This oscillating component is not present in Eq. (4.6a) because of its small magnitude ($\sim \omega$), which exceeds the accuracy of the quasiclassical approximation. The full-scale rapid oscillations of current in region VI are reduced after integration over energy and they are perfectly compensated for by the current from region V.

At finite temperature the current compensation is lifted due to the energy-dependent Fermi factor in Eq. (4.1), which yields a current of thermal excitations that is not exponentially small (with respect to eV). The smooth part of this current, resulting from noninterfering terms in Eqs. (4.6), has the form

$$I_{>}(T) = \frac{2e^2V}{\pi} \sqrt{\frac{\pi\Delta D}{2T}} e^{-\Delta/T}, \quad T/\Delta \ll D. \quad (4.10)$$

In the opposite limit the current of thermal excitations is

$$I_{>}(T) = \frac{e^2DV}{4\pi} \frac{\Delta}{T} \left(\frac{\pi}{2} - 1 \right) \cosh^{-2} \frac{\Delta}{2T}, \quad D \ll T/\Delta, 1. \quad (4.11)$$

The result of numerical evaluation of the smooth current component is plotted in Fig. 7 with dashed lines. The solid lines show the exact current of thermal excitations which manifests pronounced oscillating features. Although the accuracy of the quasiclassical approximation is not sufficient for analytical evaluation of the amplitude of current oscillations δI_{osc} , as previously explained, the oscillation period Π : $\delta I_{\text{osc}}[(\Delta/eV) + \Pi] = \delta I_{\text{osc}}(\Delta/eV)$, can easily be evaluated from Eqs. (4.7), (4.8). Since integration over energy selects the energy $E = 1$, the oscillation period is

$$\Pi = \frac{\pi}{\int_0^\pi (\pi - \phi) dE(\phi)}, \quad (4.12)$$

where $E(\phi)$ is the static Andreev bound-state spectrum, Eq. (3.6). For low transparency, Eq. (4.12) reads

$$\Pi \approx \frac{8}{D}, \quad D \ll 1.$$

In Fig. 8, the junction conductance $G = I/V$ is plotted as a function of inverse voltage. The oscillations are clearly periodic and the period does not depend on temperature. The numerical evaluation of the period is in nice agreement with Eq. (4.12).

V. TIME-DEPENDENT CURRENT

Proceeding to calculation of the time-dependent ($N \neq 0$) part of the current in Eq. (2.16), we note that the quasiclassical approximation only allows us to investigate low-frequency current harmonics, $N\omega \ll 1$. Within such an approximation one can neglect the difference between indices of coefficients of bilinear form in Eq. (2.17),

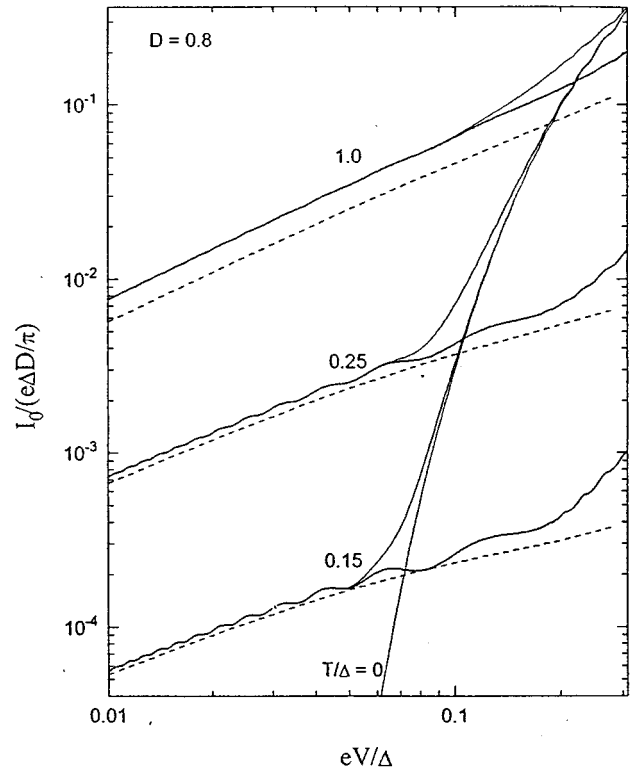
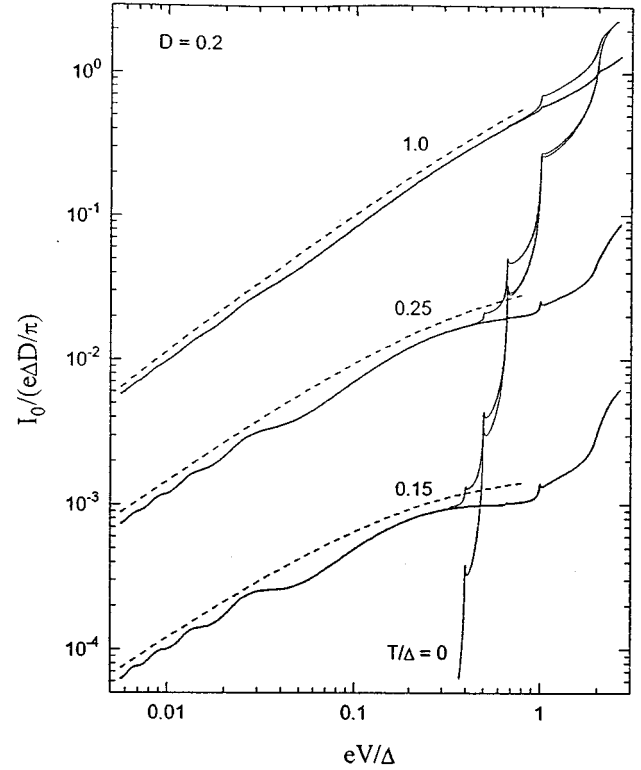


FIG. 7. I - V characteristics of junctions with transparencies $D = 0.2$ (upper) and $D = 0.8$ (lower) at different temperatures [normalized by $\Delta(T)$]. Bold lines represent exact numerical results for the current of thermal excitations (regions V - VI); dashed lines are the results of quasiclassical theory without inclusion of the interference term; thin lines show the total dc current, coinciding with the thermal excitation current at low voltage.

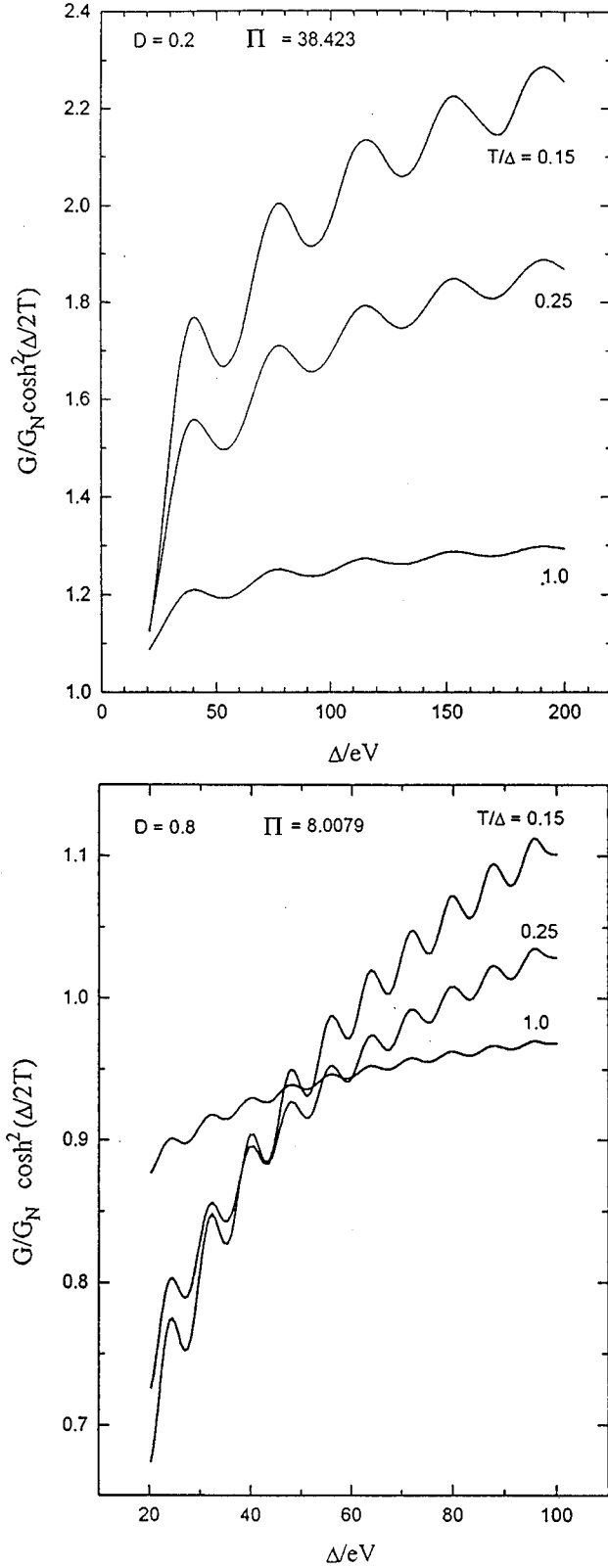


FIG. 8. Oscillations of the normalized junction conductance $G(T) = I(T)/V$ vs inverse voltage at different temperatures in junctions with transparencies $D = 0.2$ (upper) and $D = 0.8$ (lower); $G_N = e^2 D / \pi$ is the conductance of the normal junction. The period of oscillations is given by Eq. (4.12).

$$I_{ac} = \frac{e\Delta}{\pi} \sum_{N=1}^{\infty} \int_1^{\infty} \frac{dEE}{\xi} \tanh(E\Delta/2T) \times \int_{-\infty}^{\infty} \frac{d\epsilon}{\omega} 2 \operatorname{Re} [e^{iN\omega\tau} K_N(E, \epsilon)], \quad (5.1)$$

$$K_N(E, \epsilon) = \cosh[\operatorname{Re} \gamma(\epsilon)] \{ [f^*(\epsilon + N\omega) f(\epsilon) - b^*(\epsilon + N\omega) b(\epsilon)] - (\gamma \rightarrow -\gamma) \}.$$

Furthermore, when calculating products of scattering amplitudes in Eq. (5.1), we will assume coinciding arguments in the pre-exponential factors in Eq. (3.8) and expand quasiclassical exponents: $S(\epsilon + N\omega) \approx S(\epsilon) + S'N\omega$. The main contribution to the ac current at all temperatures results from regions *II* and *IV*—classically allowed regions for Andreev bound-state oscillations. The current spectral density K_N^I differs from the static Eq. (4.3) containing the additional exponential factor $\exp(S'N\omega) \approx \exp[iN\phi(\epsilon)]$:

$$K_N^I(E, \epsilon) = \frac{4\xi^2 W}{\sqrt{D}} e^{-2S(1,E)} e^{iN\phi(\epsilon)}, \quad (5.2)$$

where $\phi(\epsilon)$ is given by Eq. (3.6). The current spectral density in region *IV* only consists of incoherent contributions of incoming waves and waves reflected from the Andreev gap,

$$K_N^{IV}(E, \epsilon) = \frac{4\xi^2}{\sqrt{D}} e^{-2S(1,E)} (e^{-iN\phi(\epsilon)} - |Q|^2 e^{iN\phi(\epsilon)}) \quad (5.3)$$

(the interference current vanishes in the quasiclassical approximation). Combination of Eqs. (5.2), (5.3), and (5.1) yields the ac current,

$$I_{ac}^{II+IV} = \frac{e\Delta D}{2} \tanh \frac{\Delta}{2T} \left[(1-W) \frac{\sin \omega \tau}{\sqrt{1-D \sin^2(\omega \tau/2)}} + W \left(\frac{|\sin \omega \tau|}{\sqrt{1-D \sin^2(\omega \tau/2)}} - \frac{4(1-\sqrt{R})}{\pi D} \right) \operatorname{sgn} V \right], \quad (5.4)$$

which consists both of sine and cosine components (odd and even with respect to time reversal) and undergoes crossover from cosine-like behavior in the contact limit $D=1$ ($W=1$) to sine-like behavior in the tunnel limit $D \ll 1$ ($W \ll 1$). A similar crossover occurs with decreasing voltage when $R \ll 1$: from cosine-like behavior at comparatively large voltage, $eV \gg R\Delta$, to sine-like behavior at low voltage $eV \ll R\Delta$. We note that the instant current in Eq. (5.4) in the limit $V \rightarrow 0$ does not approach the static Josephson current, having different temperature dependence. The dc Josephson current possesses a temperature dependence $\tanh(E(\phi)\Delta/2T)$ with $E(\phi)$ given by Eq. (3.6), which reflects the equilibrium population of the static Andreev bound states. In contrast, the temperature factor in Eq. (5.4) reflects the nonequilibrium population of oscillating Andreev states through the Fermi filling factor at the gap edge $E=1$. Such a difference persists unless the period of Josephson oscillations exceeds the inelastic relaxation time.^{7,24}

The last, time-independent, term in Eq. (5.4) is equal to the zeroth harmonic of the current of regions *II, IV*, and

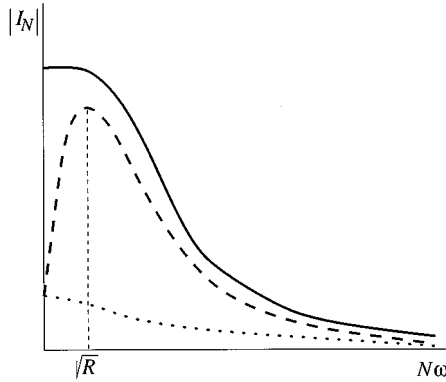


FIG. 9. Spectral distribution of the cosine harmonics of the ac Josephson current. The solid line is the fully transparent junction ($R=0$); dotted line is the junction with finite reflectivity ($R>\omega$), contribution of Andreev bound states; dashed line is the junction with finite reflectivity ($R>\omega$), total cosine current with account of contribution of the Andreev gap.

therefore represents the time-averaged magnitude of the total ac current of the oscillating quasistatic Andreev states. It was pointed out in Ref. 23 that in fully transparent junctions, $R=0$, the dc current is entirely produced by oscillating Andreev states. In junctions with finite reflectivity, $R>0$, according to Eq. (5.4) only part of dc pair current, Eq. (4.4), results from oscillating Andreev states—the remaining part is contributed by nonadiabatic states within the Andreev gap (region III).

The conclusion drawn above about the exponentially small magnitude of the cosine current in the tunnel regime concerns, rigorously speaking, only the low-frequency part of the ac current. The suppression of the low-frequency current is caused by the conservation law in Eq. (2.20), which is nearly fulfilled in this frequency region and which establishes approximate balance of the normal and Andreev currents. On the other hand, one has to expect that high-frequency harmonics are not suppressed: harmonics in the region $N\omega \gg \sqrt{R}$ should not be sensitive to the presence of a gap in the static Andreev spectrum and must approximately have the same magnitude as the cosine harmonics in fully transparent junctions, $R=0$. Such arguments lead to the spectrum of the cosine ac current sketched in Fig. 9: the amplitudes of the harmonics, being exponentially small at small N , rapidly grow with N and after approaching a maximum at $N\omega \sim \sqrt{R}$ decay with a power law, similarly to the spectrum of the transparent junction. The nonadiabatic effect of exponential growth of the harmonic amplitudes at low frequency is provided by the contribution of the forbidden region III.

The contribution of forbidden regions to the ac current is always restricted to the cosine component,

$$I_{\text{ac}} = \sum_{N=1}^{\infty} I_N \cos(N\omega\tau). \quad (5.5)$$

The current contribution of region III

$$I_N^{\text{III}} = \frac{4e\Delta W}{\pi} \tanh \frac{\Delta}{2T} (-1)^N \int_0^{\sqrt{R}} d\epsilon \cosh(N \operatorname{arccosh}|U(\epsilon)|) \quad (5.6)$$

results from the interference terms $f_+^*(\epsilon+N\omega)f_-(\epsilon)$, and other similar terms, which combine growing and decaying elementary solutions. The first harmonics in Eq. (5.6) have the same order of magnitude as the cosine current of oscillating Andreev states in Eq. (5.4). The harmonic amplitudes exponentially grow with N ,

$$I_N^{\text{III}} = \frac{4e\Delta W}{\pi} \tanh \frac{\Delta}{2T} (-1)^N \left(\frac{\pi\sqrt{R}}{N} \right)^{1/2} \times \exp(N \operatorname{arccosh}(1+2R/D)), \quad N \gg 1,$$

until $N\omega$ exceeds the size of region III, $N_{\text{max}} \sim \sqrt{R}/\omega$.

The spectral density of the ac current in region I rapidly decays with departure from the superconducting gap edge, similarly to the dc current. Therefore, its contribution is small with respect to the cosine current of the Andreev states,

$$I_{N<} = \frac{e\Delta W}{\pi} (D\omega^2)^{1/3} a_N \tanh \frac{\Delta}{2T}, \quad (5.7)$$

$$a_N = \int_0^{\infty} dx \exp\left(-\frac{2}{3}x^{3/2} - \frac{2}{3}(x+2N/N_0)^{3/2}\right),$$

$$N_0 = (D/\omega)^{1/3}.$$

The currents in regions V and VI nearly compensate each other at zero temperature, yielding a total current coinciding with the contribution of region I, $I_{N>} = I_{N<}$. At nonzero temperature the current compensation is lifted, which leads to an ac current of thermal excitations. The smooth, noninterference component of this current,

$$I_{N>}(T) = \frac{4e^2\Delta}{\pi} e^{-\Delta/T} \sqrt{D} \int_0^{\infty} \frac{dx}{x^2} (1 - e^{-2Tx^2/\Delta}) \times \exp(-2N\sqrt{D}x), T/\Delta \ll D, \quad N \ll N_0, \quad (5.8)$$

decreases with harmonic number N as N^{-1} . At $N \gg N_0$ the current harmonics decay exponentially.

We conclude this section with a remark about the sign of the cosine current (see the discussion in Ref. 35). Although the signs of all harmonics in Eq. (5.8) are positive, the sign of the total cosine current may be negative due to competition with the cosine current of the Andreev bound states in Eqs. (5.4) and (5.6). In particular, the contribution by the Andreev bound states to the first cosine harmonic is negative.

VI. CONCLUSION

In conclusion, we have calculated the dc current and the ac Josephson current in quantum superconducting junctions at low applied voltage $eV \ll \Delta$ in the whole range of junction transparency $0 < D < 1$. The global structure of multiple Andreev scattering and the distribution of currents among inelastic-scattering channels is described in terms of the wave function of an effective quasiclassical particle propagating along the energy axis.

The main physical characteristic, which determines the properties of low-biased junctions with intermediate transparency, is the energy gap in the static Andreev bound-state spectrum. Opening of the Andreev gap yields exponential

suppression of the dc current, and determines the crossover from the contact to the tunnel regime of both the dc current and the ac Josephson current as functions of junction transparency and applied voltage. Quasiparticle reflection from the edges of the Andreev gap causes mesoscopic phenomena manifested in oscillating features on current-voltage characteristics at finite temperature.

At zero temperature, the pair current always gives the main contribution to the dc current and is homogeneously distributed within the superconducting energy gap. In the tunnel regime $eV \ll R\Delta$, the suppression of the low-frequency cosine harmonics of the ac current is lifted at higher frequency: the amplitudes of the cosine harmonics grow exponentially with the harmonic number N , and achieve at $NeV \sim \sqrt{R}\Delta$ a magnitude of the order of the non-suppressed current in a pure constriction.

The present investigation has been concerned with junctions whose scattering properties in the normal state do not depend on energy, which is true for all kinds of weak links with lengths shorter than the coherence length. However, the method can be extended to long superconductor-normal-

metal-superconductor junctions, junctions with resonance tunnel barriers, and other structures where electron-hole dephasing effects are important. It has been shown in Ref. 36 that the electron-hole dephasing gives rise to modification of the spectral equation (3.6) to the form $\cos\phi = F[r(E), d(E)]$, where F is a universal function of the electron-scattering amplitudes of the normal part of the junction. Therefore, although the shape of the effective potential in the energy-domain wave equation (3.4) is specifically modified for each particular junction, the whole scenario remains unchanged.

ACKNOWLEDGMENTS

This work has been supported by the Swedish National Science Research Council (NFR), the Swedish National Board for Technical and Industrial Development (NUTEK), and the Swedish Royal Academy of Sciences (KVA). Part of the work has been supported by Grant No. INTAS-94-3861 and by the Ukrainian State Foundation for Fundamental Research, Grant No. 2.4/136.

-
- ¹T.M. Klapwijk, G.E. Blonder, and M. Tinkham, *Physica B+C* **109-110**, 1657 (1982).
- ²M. Octavio, M. Tinkham, G.E. Blonder, and T.M. Klapwijk, *Phys. Rev. B* **27**, 6739 (1983).
- ³R. Kümmel and W. Senftinger, *Z. Phys. B* **59**, 275 (1985).
- ⁴G.B. Arnold, *J. Low Temp. Phys.* **68**, 1 (1987).
- ⁵K. Flensberg, J. Bindslev Hansen, and M. Octavio, *Phys. Rev. B* **38**, 8707 (1988).
- ⁶R. Kümmel, U. Gunsenheimer, and R. Nicolisky, *Phys. Rev. B* **42**, 3992 (1990).
- ⁷U. Gunsenheimer and A.D. Zaikin, *Phys. Rev. B* **50**, 6317 (1994).
- ⁸N.R. Werthamer, *Phys. Rev.* **147**, 255 (1966).
- ⁹J.R. Schrieffer and J.W. Wilkins, *Phys. Rev. Lett.* **10**, 17 (1963); J.W. Wilkins, in *Tunneling Phenomena in Solids*, edited by E. Burstein and S. Lundquist (Plenum, New York, 1969) p. 333.
- ¹⁰B.N. Taylor and E. Burstein, *Phys. Rev. Lett.* **10**, 14 (1963).
- ¹¹J.M. Rowell, *Rev. Mod. Phys.* **36**, 215 (1963).
- ¹²C.L. Foden, R. Rando, A. van Dordrecht, A. Peacock, J. Lumley, and C. Pereira, *Phys. Rev. B* **47**, 3316 (1993).
- ¹³R. Cristiano, L. Frunzio, R. Monaco, C. Nappi, and S. Pagano, *Phys. Rev. B* **49**, 429 (1994).
- ¹⁴A.W. Kleinsasser, R.E. Miller, W.H. Mallison, and G.B. Arnold, *Phys. Rev. Lett.* **72**, 1738 (1994).
- ¹⁵E.N. Bratus', V.S. Shumeiko, and G. Wendin, *Phys. Rev. Lett.* **74**, 2110 (1995).
- ¹⁶N. van der Post, E.T. Peters, I.K. Yanson, and J.M. van Ruitenbeek, *Phys. Rev. Lett.* **73**, 2611 (1994).
- ¹⁷E. Scheer, P. Joyez, M.H. Devoret, D. Esteve, and C. Urbina (unpublished).
- ¹⁸H. Takayanagi, T. Akazaki, and J. Nitta, *Phys. Rev. Lett.* **75**, 3533 (1995).
- ¹⁹R. Landauer, *IBM J. Res. Dev.* **1**, 223 (1957).
- ²⁰Y. Imry, *Directions in Condensed Matter Physics* (World Scientific, Singapore, 1986), p. 102.
- ²¹V.S. Shumeiko, E.N. Bratus', and G. Wendin, *Low Temp. Phys.* **23**, 249 (1997).
- ²²N. van der Post (private communication).
- ²³D. Averin and A. Bardas, *Phys. Rev. Lett.* **75**, 1831 (1995).
- ²⁴J.C. Cuevas, A. Martin-Rodero, and A. Levy Yeyati, *Phys. Rev. B* **54**, 7366 (1996).
- ²⁵E.N. Bratus', V.S. Shumeiko, E.V. Bezuglyi, and G. Wendin, *Low Temp. Phys.* **22**, 474 (1996).
- ²⁶L.I. Glazman, G.B. Lesovik, D.E. Khmel'nitskii, and R.I. Shekhter, *Pis'ma Zh. Éksp. Teor. Fiz.* **48**, 218 (1988) [*JETP Lett.* **48**, 238 (1988)].
- ²⁷P.G. de Gennes, *Superconductivity of Metals and Alloys* (Addison-Wesley, New York, 1989).
- ²⁸V.S. Shumeiko, G. Wendin, and E.N. Bratus', *Phys. Rev. B* **48**, 13 129 (1993).
- ²⁹I.O. Kulik and A. N. Omel'yanchuk, *Fiz. Nisk. Temp.* **3**, 945 (1977); **4**, 296 (1978) [*Sov. J. Low Temp. Phys.* **3**, 459 (1977); **4**, 142 (1978)].
- ³⁰I.O. Kulik, R.I. Shekhter, and A.N. Omel'yanchouk, *Solid State Commun.* **23**, 301 (1977).
- ³¹V.P. Galaiko, *Zh. Éksp. Teor. Fiz.* **61**, 382 (1971) [*Sov. Phys. JETP* **34**, 203 (1972)].
- ³²S.V. Kuplevakhskii and I.I. Fal'ko, *Fiz. Nizk. Temp.* **17**, 961 (1991) [*Sov. J. Low Temp. Phys.* **17**, 501 (1991)].
- ³³A. Furusaki and M. Tsukada, *Physica B* **165-166**, 967 (1990).
- ³⁴M. Abramovits and I.A. Stegun, *Handbook of Mathematical Functions*, Appl. Math. Series 55 (National Bureau of Standards, 1968).
- ³⁵A. Barone and G. Paterno, *Physics and Applications of the Josephson Effect* (Wiley, New York, 1982).
- ³⁶G. Wendin and V.S. Shumeiko, *Superlattices Microstruct.* **20**, 569 (1996).